Climatic variability over time scales spanning nine orders of magnitude: connecting Milankovitch cycles with Hurst-Kolmogorov dynamics

Yannis Markonis and Demetris Koutsoyiannis*

Department of Water Resources and Environmental Engineering, Faculty of Civil Engineering, National Technical University of Athens, Heroon Polytechneiou 5, GR 157 80 Zographou, Greece

* Corresponding author: dk@itia.ntua.gr – http://www.itia.ntua.gr/dk

Manuscript submitted to *Geophysical Research Letters*

August 2011

Abstract We investigate climatic variability using two instrumental series of global temperature and eight proxy series with varying lengths from 2 thousand to 500 million years. By superimposing the climacograms (logarithmic plots of standard deviation versus time scale) of the different series we obtain an impressive overview of the variability for time scales spanning almost 9 orders of magnitude—from 1 month to nearly 100 million years. An overall climacogram slope of –0.08 supports the presence of Hurst-Kolmogorov dynamics with Hurst coefficient of at least 0.92. The orbital forcing (Milankovitch cycles) is also evident in the combined climacogram at time scales between 10 and 100 thousand years. While orbital forcing favors predictability at the scales it acts, the overview of climate variability at all scales suggests a big picture of enhanced change and enhanced uncertainty of Earth's climate.

1. Introduction

In the first half of 19th century, geologic evidence indicated that at least one glacial period existed in Earth's geologic history (Agassiz, 1840; from Imbrie, 1982). In the following decades it became clear that during the Pleistocene (2 588 000 – 12 000 years BP), there were many glacial periods followed by shorter interglacials, such as the one we experience since the onset of human civilization. Milankovitch (1941) provided an explanation of these recurring glaciations/deglaciations based on Earth's orbit variations, which was confirmed after some years by the first temperature reconstructions.

Additional findings showed that the climate during the Holocene (the last 12 000 years), earlier regarded static, was characterized by many climatic events, such as 'Little Ice Age', 'Medieval Warm Period', 'Younger Dryas cold episode', 'Holocene Optimum', '8 200 Holocene Event' and 'Bond Events', deviating from 'normal' conditions for hundreds or thousands of years (Bond et al., 2001). These events cannot be attributed to the Milankovitch cycles, whose periods are much longer (i.e. 21, 41 and 100 thousand years for the precession, obliquity and eccentricity cycles, respectively). Furthermore, it is well known that succession of glaciation and deglaciation periods has not occurred all the time, but only during large periods called ice ages, such as the current (Pliocene-Quaternary) ice age that started about 2.5 million years ago, as well as the Ordovician and the Carboniferous ice ages each of which lasted almost 100 million years (Crowell and Frakes, 1970).

Thus, it is very difficult to attribute the climate variability, both at multi-decadal and multi-million-year scales to specific quantifiable causal mechanisms that would be applicable all the time. A more modest goal, which is the purpose of this study, would be to characterize this variability over the widest possible range of scales that the available evidence allows. Such characterization unavoidably uses stochastic descriptions and tools, but without neglecting identifiable deterministic controls, such as the Milankovitch cycles.

2. Data

Ten temperature-related time series with time steps spanning from monthly to 500 thousand years and overall lengths from 30 years to 500 million years are used in this study, as summarized in Table 1. Two of the time series are instrumental, based on satellite (NSSTC) and ground (CRU) data. All others are reconstructions of three types, i.e. (a) annual-scale, multi-proxy, global temperature reconstructions (Moberg, based on tree-rings, boreholes, cave stalagmites and sediment data, and Lohle, which adds pollen data but leaves out tree ring data); (b) proxy data extracted from one-site ice cores (EPICA, GRIP, and Taylor Dome); and (c) multi-site ocean sediment depositions (Huybers, Zachos and Veizer). To reduce the within-year variability, the two instrumental time series, whose step is monthly, refer to temperature deviations from the 30-year monthly average. The ice-core and sediment reconstructions had varying time step and were converted by linear interpolation to constant time step, not greater than the varying raw time step. To maintain a satisfactory sample size, in the cases of Taylor and GRIP reconstructions we used only the highest resolution fraction of each time series.

As observed in Figure 1, climatic change is evident at all scales. The most important events in the last 500 million years are the ice ages described above (seen in the Veizer time series as low-temperature periods). A decreasing trend in global temperature has been prevailing in the last 50 million years (Zachos reconstruction), while in the last 2.5 million the oscillating pattern of glaciers extension and retreat have emerged (Huybers time series, also seen in EPICA and GRIP data). The frequency of these quasi-cycles correlates well with the frequencies of Earth's orbital parameters, which affect the incoming insolation providing a possible connection between the glaciation process and orbital forcing (Milankovitch, 1941). Till now many efforts have been done to describe the exact physical mechanism of this connection, but their results are still under debate (Paillard, 1998; Huybers and Wunsch, 2005; Roe, 2006). In the interglacial of the last 12 000 years, climatic fluctuations are weaker

(Taylor Dome ice core) than in the earlier glaciation period (GRIP data). However as we move to even smaller scales (Moberg, Lohle and instrumental series), deviations from the average become again apparent.

3. Climate variability at different time scales

By its definition, climate involves averaging of a continuous time process $\underline{x}(t)$ at various time scales k. This transforms the instantaneous-time process $\underline{x}(t)$ into a discrete time process $\underline{x}_i^{(k)}$ at time i and scale k, i.e.

$$\underline{x}_i^{(k)} := \frac{1}{k} \int_{(i-1)k}^{ik} \underline{x}(t) dt \qquad (1)$$

The climatic variability is naturally quantified by the standard deviation $\sigma^{(k)}$ of $\underline{x}_i^{(k)}$. A key tool that provides a multi-scale stochastic characterization is the plot (typically double logarithmic) of $\sigma^{(k)}$ versus k, which has been termed the climacogram (from the Greek climax, i.e., scale). The climacogram is simpler and more robust than other commonly used stochastic tools, the power spectrum and the autocorrelogram, although it is related to them by simple transformations (Koutsoyiannis, 2010). In addition, as will be seen below, the climacogram is very powerful, offering means to combine views of different time series in a single graph.

A fully deterministic, strictly periodic process with period T, described by

$$x(t) = \sqrt{2} \cos(2\,\pi\, t \,/\, T + b) \qquad (2)$$

if treated stochastically will have marginal density function $f(x) = 1/(\pi\sqrt{2 - x^2})$, mean 0, variance 1, and autocovariance $c(\tau) = \mathrm{cov}[x(t), x(t + \tau)] = \cos(2\,\pi\,\tau \,/\, T)$, which does not depend on t. It is then readily showed that its climacogram is

$$\sigma^{(k)} = [T \,/\, (\pi\, k)]\; |\sin(\pi\, k/T)| \qquad (3)$$

It is easily seen from (3) that for $k << T$, the standard deviation is constant, $\sigma^{(k)} = 1$, while for $k > T$ the climacogram has a series of peaks on points $k = (n + 1/2)T$, over which $\sigma^{(k)} = T \,/\, (\pi\, k)$.

Assuming that the real climate is affected by a multitude of cycles, where no periodicity T is a priori excluded, the resulting composite process will have a climacogram that could be determined by adding partial climacograms of the form (3) for each T. Superposition of fluctuations occurring at many time scales (caused, e.g., by orbital forcing, solar irradiance, volcanic activity and so forth) tends to give a composite process with Hurst-like properties (Koutsoyiannis, 2003). Moreover, extremal entropy production considerations result in a process with a climacogram given by the simple power-law relationship

$$\sigma^{(k)} = k^{H-1}\,\sigma \tag{4}$$

where $\sigma^{(k)}$ is the standard deviation at time scale k (with $\sigma \equiv \sigma^{(1)}$) and H is the entropy production in logarithmic time (Koutsoyiannis, 2011). The constant H is more commonly known as the Hurst coefficient after Hurst (1951) who was the first to verify the scaling behavior (4) in natural processes, describing it as the tendency of extreme events (like Nile's floods or droughts) to cluster in time. A mathematical process having the property (4) was first studied by Kolmogorov (1940).

Thus, (4) represents a natural behavior, defines a stochastic process with this behavior, and describes the stochastic dynamics of this process. Here we use the term Hurst-Kolmogorov (HK) as a collective name to describe the natural behavior (which for H in (0.5, 1) is also known as the Hurst phenomenon, long term persistence or long range dependence), the stochastic process (also known as a fractional Gaussian noise or simple scaling process) and the stochastic dynamics. The common white noise process, which is characterized by independence in time, is a specific case of the HK process, in which $H = 0.5$, so that $\sigma^{(k)} = \sigma/k^{0.5}$ (which implies a slope of –0.5 in the climacogram). In real-world time series H is usually greater than 0.5 (with slopes milder than –0.5). HK dynamics with $H > 0.5$ has been already identified in some individual temperature reconstructions (Bloomfield, 1992; Richards, 1994; Ashkenazy et al., 2003; Koutsoyiannis and Montanari, 2007; Koutsoyiannis et al., 2009).

4. Application, results and discussion

Each of the ten data series allows the construction of an empirical climacogram based on the classical sample estimates of the standard deviation $\sigma^{(k)}$ for aggregate scales k spanning from the available resolution Δ (shown in Table 1) up to, say, $k = L/10$ (with L being the total length of the time series shown in Table 1), so that at least 10 data points are available to estimate $\sigma^{(k)}$. We can then superimpose all climacograms of the ten time series to construct a combined climacogram representative for time scales ranging from monthly to 50 million years. Since the units of the various series differ, those of standard deviations will differ too. Also, each data point of a proxy series does not necessarily represent the time average at the specific scale. For these reasons, the climacograms of the different series are not fully compatible to each other. However, here we are interested about the variation of standard deviation with scale, rather than the precise values of standard deviation. Thus we can multiply each climacogram by a constant value, so us to match the different climacograms. In the logarithmic plot of Figure 2, this entails a translation of the climacogram of each time series, which obviously does not affect the slopes of climacograms.

In the combined empirical climacogram of Figure 2, we have arbitrarily set $\sigma^{(k)} = 1$ for $k =$ 1 month (1/12 year). The combined climacogram gives us an impressive overview of climatic variability spanning almost 9 orders of magnitude—from 1 month to nearly 100 million years. We observe that the $\sigma^{(k)}$ of all series and all scales k are kept high, within one order of magnitude (between 0.1 and 1), as contrasted to a pure random climate, that would entail a climacogram quickly descending (with slope –0.5, also depicted in Figure 2) to lower orders of magnitude. Overall, the combined climacogram indicates a mild slope of about –0.08, suggesting a strong HK behavior. A slope of –0.08 in a theoretical climacogram would correspond to $H = 0.92$, but here the climacogram is empirical and thus possibly negatively biased (Koutsoyiannis, 2003). Thus, we can regard the value 0.92 as a lower bound of H. However, even H = 0.92 is a very high value and implies spectacular differences from the classical statistics (in which the consecutive values are independent), as well as from typical stochastic processes like the Markov (AR(1)) process. Classical statistics has served as the common basis of thinking, understanding and interpreting climate behaviors, and performing statistical tasks such as estimation and hypothesis testing. The horizontal line in Figure 2 (drawn from the rightmost point of the sloped straight line fitted to the empirical climacogram) demonstrates that the real climatic variability at the scale of 100 million years equals that predicted by classical statistics for 28 months (!). This dramatic difference, suggestive of enhanced change and enhanced unpredictability, should help us understand that the classical statistical thinking may be inappropriate for climate and that the classical dichotomy, implied by classical statistical thinking, of weather versus climate may be misleading.

Furthermore, the combined climacogram suggests a departure from the simple scaling HK law for scales between 10 and 100 thousand years, where the slope is steeper than –0.08, up to around –0.5. The explanatory toy model of Figure 3 helps understand that this is the result of the Milankovitch cycles acting at this range of time scales. This toy model represents the synthesis of the theoretical climacograms of three components, an HK process with H = 0.92 and two harmonics with periods 100 and 41 thousand years; the composite climacogram is readily calculated from (3) and (4). Clearly, as a result of the two harmonics, the climacogram slope at scales between 10 and 100 thousand years is much steeper than –0.08, as in the real-world climacogram.

Several “imperfections” can be observed in the matching of the climacograms of the different time series in Figure 2. These are not unexpected, and they themselves are the result of the bias and enhanced uncertainty implied by the long-term persistence in statistical estimation. In some cases, the right tail of a climacogram is too flat, as for example in Zachos and CRU time series. The reason for a flat tail is related to the fact that the entire time series length is located on a branch of the process with a monotonic trend (Figure 1). When a longer time series is viewed (Veizer for Zachos, Moberg and Lohle for CRU), which shows that the monotonic trend is in fact part of a longer fluctuation, the flat climacogram problem is remedied.

One of the most prominent “imperfections” of Figure 2 is related to the EPICA climacogram, whose right tail has a slope steeper than –0.5, which could be interpreted as indicating anti-persistence. However, this behavior can be easily attributed to the combined effect of statistical bias and the influence of the orbital forcing. To demonstrate this we have used the toy model of Figure 3 to generate a series with resolution and length equal to those of the EPICA series. The resulting empirical climacogram, also plotted in Figure 3, resembles the real EPICA climacogram of Figure 2.

Generally, the steeper slope at time scales between 10 and 100 thousand years suggests higher predictability over those scales in comparison to shorter or longer scales, but again this does not counteract the enhanced uncertainty and unpredictability entailed by the overall HK dynamics. This uncertainty is magnified by the fact that, as already mentioned, the orbital forcing cycles are not apparent all the time and are not strictly periodic (see also Richards, 1994; Ashkenazy et al., 2003). Endeavors to describe the climatic variability in deterministic terms are equally misleading as those to describe it using classical statistics. Connecting deterministic controls, such as the Milancovich cycles, with the Hurst-Kolmogorov stochastic dynamics seems to provide a more promising path for understanding and describing climate.

References

Agassiz, L. (1840), *Etudes sur les glaciers*, Privately published, Neuchatel.

Ashkenazy, Y., D. R. Baker, H. Gildor, and S. Havlin (2003), Nonlinearity and multifractality of climate change in the past 420 000 years, *Geoph. Res. L.*, *30*(22), 2146, doi:10.1029/2003GL018099.

Bloomfield, P. (1992), Trends in global temperature, *Clim. Change*, *21*, 1-16.

Bond, G., Kromer, B., Beer, J., Muscheler, R., Evans, M. N., Showers, W., Hoffmann, S., et al. (2001), Persistent solar influence on north Atlantic climate during the Holocene, *Science*, 294(5549), 2130-2136. doi:10.1126/science.1065680

Brohan, P., J. Kennedy, I. Harris, S.F.B. Tett, and P. Jones (2010), Uncertainty estimates in regional and global observed temperature changes: a new dataset from 1850, *J. Geophys. Res.*, *111*, D12106, doi:10.1029/2005JD006548.

Crowell, J. C., and L. A. Frakes (1970), Phanerozoic glaciation and the causes of ice ages, *Am. J. Sc.*, *268*, 193-224, doi:10.2475/ajs.268.3.193.

Dansgaard, W., and GRIP Scientific Team (1993), Evidence for general instability in past climate from a 250-kyr ice-core record. *Nature*, *364*, 218-220.

Hurst, H. E. (1951), Long term storage capacities of reservoirs, *Trans. Am. Soc. Civil Engrs.*, *116*, 776-808.

Huybers, P. (2007), Glacial variability over the last two million years: an extended depth-derived age model, continuous obliquity pacing, and the Pleistocene progression, *Quat. Sci. Rev.*, *26*(1-2), 37-55.

Huybers, P., and C. Wunsch (2005), Obliquity pacing of the late Pleistocene glacial terminations, *Nature*, *434*(7032), 491-494.

Imbrie, J. (1982), Astronomical theory of the Pleistocene ice ages: A brief historical review, *Icarus*, *50*(2-3), 408-422.

Jouzel, J., and EPICA Scientific Team (2007), *EPICA Dome C Ice Core 800KYr Deuterium Data and Temperature Estimates*, IGBP PAGES/World Data Center for Paleoclimatology, 2007-091, NOAA/NCDC Paleoclimatology Program, Boulder, Co.

Kolmogorov, A. N. (1940), Wienersche Spiralen und einige andere interessante Kurven in Hilbertschen Raum, *Dokl. Akad. Nauk URSS*, *26*, 115-118.

Koutsoyiannis, D. (2003), Climate change, the Hurst phenomenon, and hydrological statistics, *Hydrol. Sci. J.*, *48*(1), 3-24.

Koutsoyiannis, D. (2010), A random walk on water, *Hydrol. Earth Syst. Sci.*, *14*, 585–601,.

Koutsoyiannis, D. (2011), Hurst-Kolmogorov dynamics as a result of extremal entropy production, *Physica A*, *390*(8), 1424–1432.

Koutsoyiannis, D. and A. Montanari (2007), Statistical analysis of hydroclimatic time series: Uncertainty and insights. *Water Resour. Res.*, *43*(5), 1-9.

Koutsoyiannis, D., A. Montanari, H. F. Lins, and T.A. Cohn (2009), Climate, hydrology and freshwater: towards an interactive incorporation of hydrological experience into climate research—DISCUSSION of "The implications of projected climate change for freshwater resources and their management", *Hydrol. Sci. J.*, *54*(2), 394–405.

Lohle, C. (2007), A 2000-year global temperature reconstruction based on non-treering proxies, *Energy Environ.*, *18*(7-8), 1049-1058.

Milankovitch, M. (1941), Kanon der Erdbestrahlung und seine Andwendung auf das Eiszeitenproblem, *Royal Serbian Academy Special Publication*, *133*, Belgrade. [English version published by the Israel Program for Scientific Translations, Jerusalem, 1969.]

Moberg A., D. Sonechkin, K. Holmgren, N. Datsenko, and W. Karlén (2005), Highly variable Northern Hemisphere temperatures reconstructed from low- and high-resolution proxy data, *Nature*, *433*(7026), 613-617.

Paillard, D. (1998), The timing of Pleistocene glaciations from a simple multiple-state climate model, *Nature*, *391*(6665), 378-381.

Richards, G. R. (1994), Orbital forcing and endogenous interactions: Non-linearity, persistence and convergence in late Pleistocene climate, *Quaternary Science Reviews*, *13*(8), 709-725.

Roe, G. (2006), In defense of Milankovitch, *Geophys. Res. L.*, *33*(24), L24703, doi:10.1029/2006GL027817.

Steig, E. J., D. L. Morse, E. D. Waddington, M. Stuiver, P. M. Grootes, P. A. Mayewski, M. S. Twickler, and S. I. Whitlow (2000), Wisconsinan and Holocene climate history from an ice core at Taylor Dome, Western Ross Embayment, Antarctica, *Geografiska Annaler: Series A*, *Phys. Geography*, *82*, 213-235.

Veizer, J., D. Ala, K. Azmy, P. Bruckschen, D. Buhl, F. Bruhn, G. A. F. Carden, A. Diener, S. Ebneth, Y. Godderis, T. Jasper, C. Korte, F. Pawellek, O. Podlaha, and H. Strauss (2000), 87Sr/86Sr, d13C and d18O evolution of Phanerozoic seawater. *Chem. Geology*, *161*, 59-88.

Zachos, J., M. Pagani, L. Sloan, E. Thomas, and K. Billups (2001), Trends, rhythms, and aberrations in global climate 65 Ma to present, *Science*, *292*(5517), 686-693.

Figure Captions

Figure 1 Global temperature series of instrumental data and reconstructions, described in Table 1, in different time scales, going back up to about 500 million years BP. The dashed rectangles provide the links of the time period of each time series with the one before it.

Figure 2 Combined climacogram of the ten temperature observation series and proxies. Data series with variable time step were interpolated to the time step shown in Table 1. NSSTC and CRU refer to differences of monthly global temperature to 30 year monthly average.

Figure 3 Theoretical climacograms of an HK process with H = 0.92 and two periodic processes with periods 100 and 41 thousand years, all having unit standard deviation at monthly scale, along with the climacogram of the weighted sum of these three components with weights 0.95, 0.30 and 0.15, respectively; the empirical climacogram of a synthetic time series generated from the composite process with time step and length equal to those of the EPICA series is also plotted.

Table 1. Time series of global temperature based on instrumental and proxy data.

Abbreviation	Type of data (unit)	Total length, L (years)	Resolution, Δ (years)	Reference	Data availability from
NSSTC	Satellite (^{o}C)	32	1/12		www.nsstc.uah.edu/ data/msu/t2lt/
CRU	Instrumental (^{o}C)	161	1/12	Brohan et al. (2010)	www.cru.uea.ac.uk/cru/data/temperature/
Moberg	Multi-proxy (^{o}C)	2×10^{3}	1	Moberg (2005)	www.ncdc.noaa.gov/paleo/pubs/moberg2005/moberg2005.html
Lohle	Multi-proxy (^{o}C)	2×10^{3}	30*	Lohle (2007)	www.ncasi.org/programs/areas/climate/LoehleE&E2007.csv
Taylor	Single-proxy ice core (δ^{18}O)	10×10^{3}	100	Steig et al. (1999)	nsidc.org/data/docs/agdc/nsidc0315_ahn/index.html
GRIP	Single-proxy ice core (δ^{18}O)	100×10^{3}	10	Dansgaard et al. (1993)	www.ncdc.noaa.gov/paleo/icecore/greenland/summit/document/gripisot.htm
EPICA	Single-proxy ice core (^{o}C)	800×10^{3}	500	Jouzel et al. (2007)	www.ncdc.noaa.gov/paleo/pubs/jouzel2007/jouzel2007.html
Huybers	Multi-proxy sediment (δ^{18}O)	2.6×10^{6}	10^{3}	Huybers (2007)	www.people.fas.harvard.edu/~phuybers/Progression/Averages.txt
Zachos	Multi-proxy sediment (δ^{18}O)	65×10^{6}	50×10^{3}	Zachos et al. (2001)	www.ncdc.noaa.gov/paleo/metadata/noaa-ocean-8674.html
Veizer	Multi-proxy sediment (^{o}C)	480×10^{6}	500×10^{3}	Veizer et al. (2000)	mysite.science.uottawa.ca/jveizer/isotope_data/index.html

*Scales of 1 to 30 years were not included because the series is smoothed by Lohle (2007) at the 30-year scale.

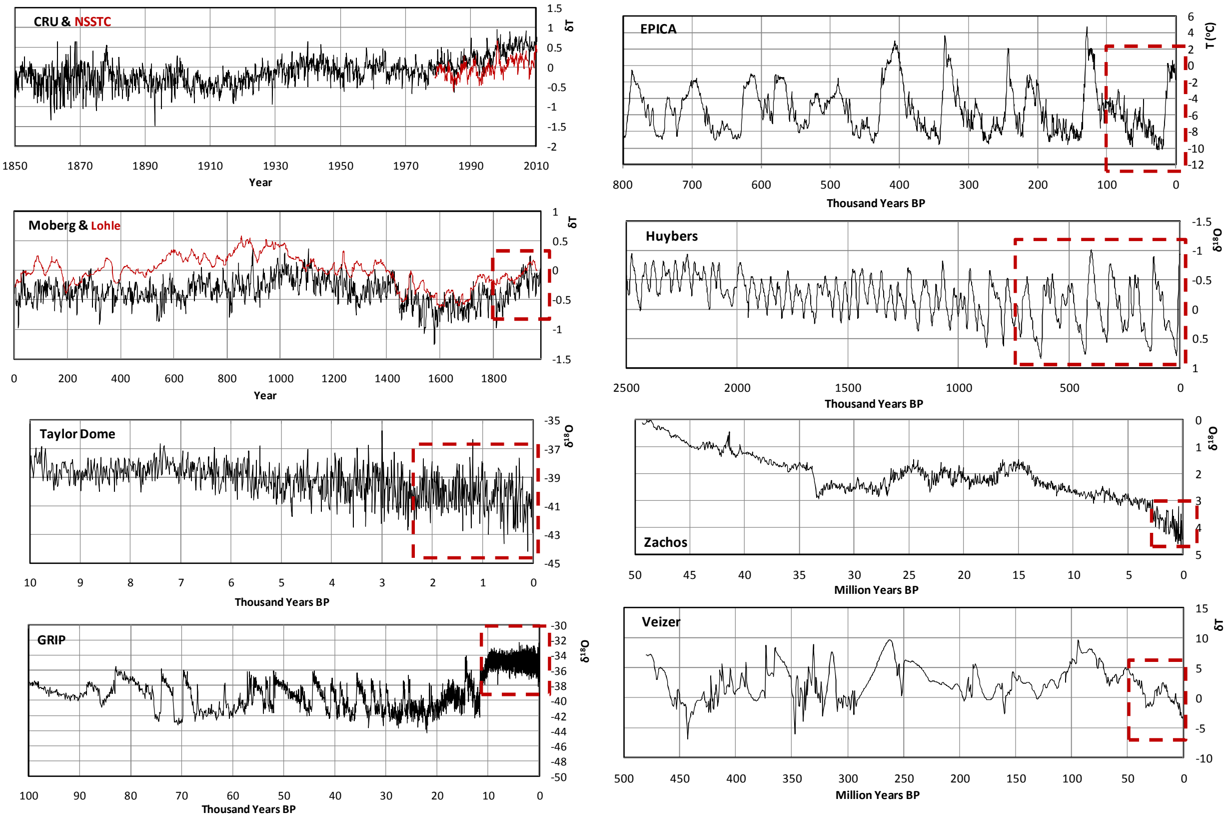

Figure 1 Global temperature series of instrumental data and reconstructions, described in Table 1, in different time scales, going back up to about 500 million years BP. The dashed rectangles provide the links of the time period of each time series with the one before it.

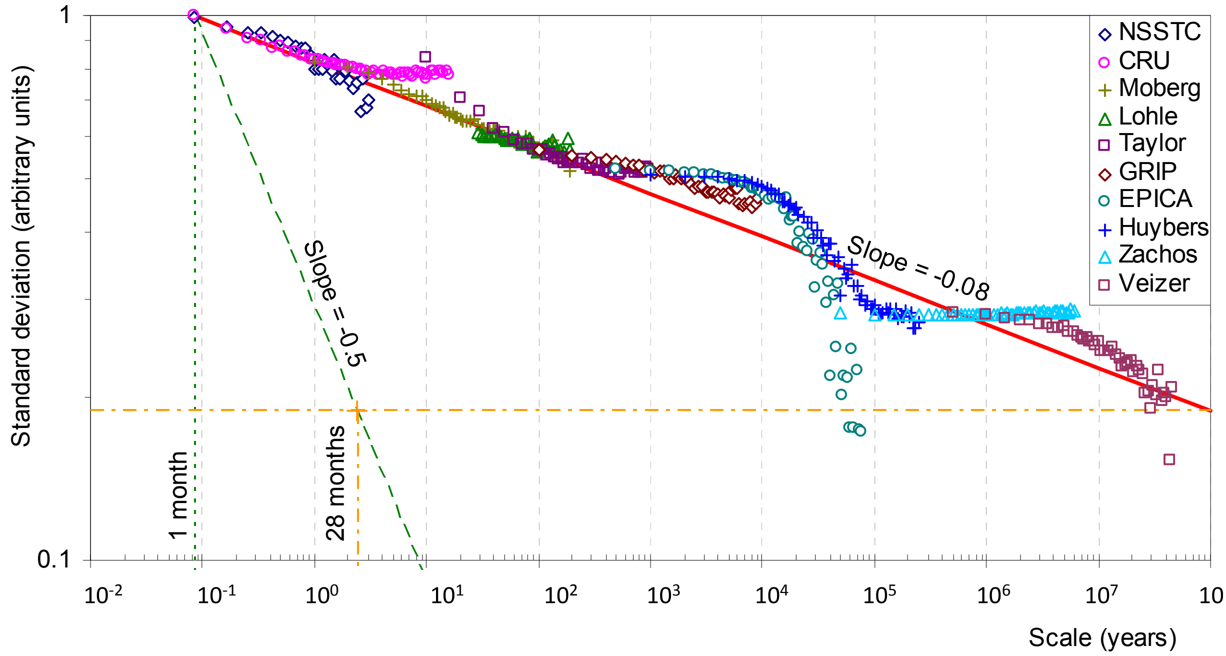

Figure 2 Combined climacogram of the ten temperature observation series and proxies. Data series with variable time step were interpolated to the time step shown in Table 1. NSSTC and CRU refer to differences of monthly global temperature to 30 year monthly average.

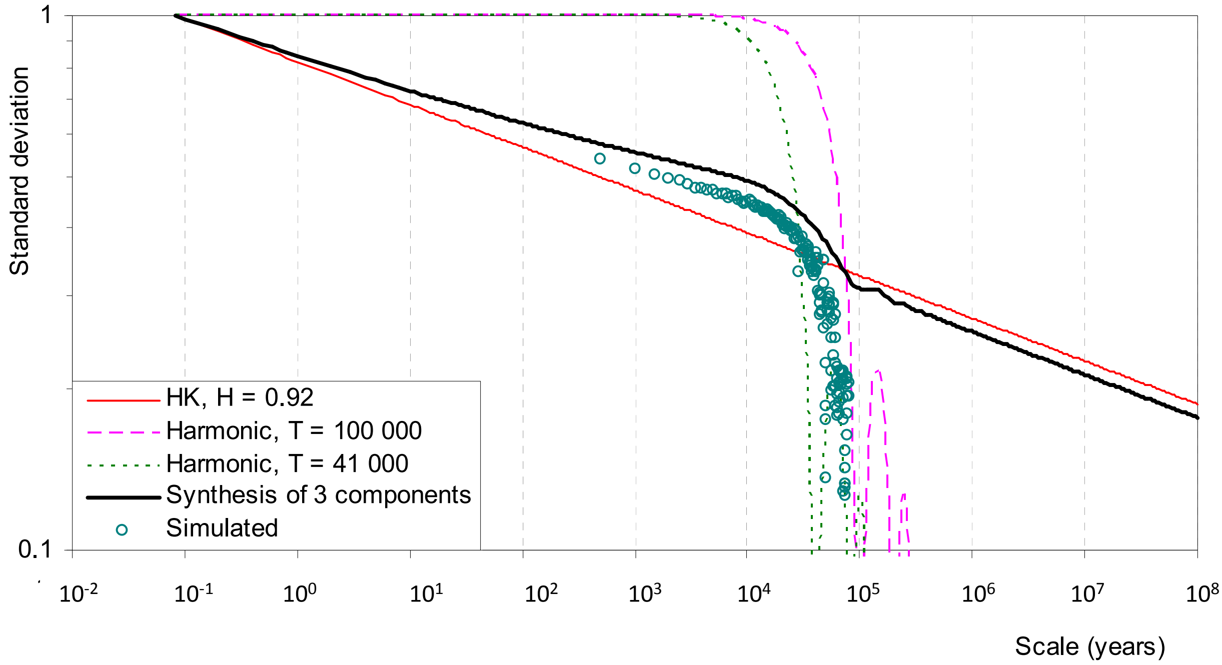

Figure 3 Theoretical climacograms of an HK process with H = 0.92 and two periodic processes with periods 100 and 41 thousand years, all having unit standard deviation at monthly scale, along with the climacogram of the weighted sum of these three components with weights 0.95, 0.30 and 0.15, respectively; the empirical climacogram of a synthetic time series generated from the composite process with time step and length equal to those of the EPICA series is also plotted.